Macromolecules

pubs.acs.org/Macromolecules Article

Confined Polymerization in Microphase-Separated Liquid Crystalline Films: Alignment-Controlled Growth of Conjugated Poly(diacetylene) Nanostructures

Sadayuki Asaoka,* Satoru Tamaki, Seiya Yokogi, Shinichi Sakurai, and Tomokazu Iyoda

Cite This: https://doi.org/10.1021/acs.macromol.5c02107 Read Online

ACCESS | Metrics & More | Article Recommendations | Supporting Information

ABSTRACT: We report the synthesis and structural characterization of side-chain liquid crystalline polymers incorporating 1,4-diphenylbuta-1,3-diyne moieties via atom transfer radical polymerization. By optimization of the polymerization conditions to circumvent radical-trapping by the diacetylene units, well-defined homopolymers and block copolymers were successfully obtained. The polymer thin films having uniaxially aligned 1,4-diphenylbuta-1,3-diyne moieties were fabricated on rubbed polyimide layers, and their orientational order was confirmed by polarized optical microscopy and UV−vis absorption spectroscopy, with high dichroic ratios and order parameters indicating strong molecular alignment. Grazing-incidence wide- and small-angle X-ray scattering revealed temperature-dependent lamellar (smectic layer) structures and the formation of hexagonally packed cylindrical microphase-separated morphologies in the block copolymers. Upon UV irradiation, polarized absorption measurements indicated that polymerization of the diacetylene units proceeded preferentially perpendicular to the rubbing direction. Time-dependent spectral shifts suggested the formation of highly conjugated poly(diacetylene) backbones with substantial molecular weights. Density functional theory calculations of model oligomers supported the experimental observations, correlating absorption features with backbone geometry and transition dipole moment orientation. Transmission electron microscopy of delaminated films confirmed that the confined polymerization preserved the internal nanostructure, maintaining a cylindrical morphology with minimal disruption. These results highlight a versatile strategy for constructing hierarchically ordered, π-conjugated polymer films by integrating liquid crystalline alignment, phase-separated architectures, and controlled solid-state polymerization.

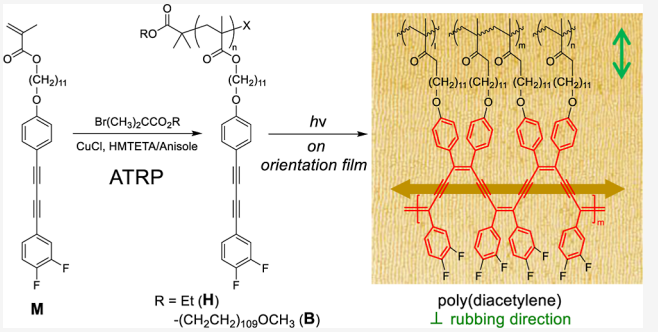

INTRODUCTION

Liquid crystal molecules exhibiting high birefringence are anticipated to find broad application in advanced optical materials, including telecommunication devices,[1] circularly polarized reflective films,[2] laser-emitting films,[3,4] and holographic media.[5] Among such compounds, tolane derivatives[6,7] and 1,4-diphenylbuta-1,3-diyne derivatives,[8−11] characterized by their linear structures and direct conjugation between aromatic rings and acetylenic units, are known for their exceptionally high birefringence. However, due to their low molecular weight and intrinsic fluidity, these small-molecule liquid crystals are typically utilized in encapsulated cell configurations. In contrast, polymerizing these high-birefringence molecules would allow for direct substrate coating or the formation of free-standing films, thereby greatly expanding their utility in device fabrication. To this end, various side-chain liquid crystalline polymers incorporating 1,4-diphenylbuta-1,3-diyne moieties as mesogenic units have been synthesized. For instance, Arakawa and co-workers reported the successful anionic polymerization of methacrylate monomers bearing 1,4-diphenylbuta-1,3-diyne groups introduced via ester linkages through alkyl chains, using *n*-butyllithium (*n*-BuLi) as an initiator.[12] The resulting polymer exhibited a weight-average molecular weight of 13,500 Da, a polydispersity index (PDI) of 1.69, and a high birefringence (Δn_0 = 0.41). Although radical polymerization is a more accessible and versatile method compared to anionic polymerization—being less sensitive to moisture and oxygen—Ogawa et al. reported that acrylates and methacrylates containing diacetylene groups tend to trap propagating vinyl radicals, thereby hindering the formation of high-molecular-weight polymers via radical pathways.[13−15] To circumvent this issue, Lu and colleagues proposed a postpolymerization modification strategy: esterification of preformed poly(methacryloyl chloride) with sodium alkoxide-terminated side-chain mesogens. This ap-

Received: August 1, 2025
Revised: October 3, 2025
Accepted: October 16, 2025

proach enabled side-chain incorporation efficiencies ranging from 30% to 70%.[16]

Atom transfer radical polymerization (ATRP), a form of controlled/living radical polymerization, mitigates side reactions by reversibly converting active chain ends into dormant species via reversible covalent bonding.[17−20] This dormant-active equilibrium has become a foundational concept for achieving controlled polymerizations and has recently gained traction as a powerful technique for synthesizing functional polymers with complex architectures.[21−24] In this study, we hypothesize that employing ATRP for the polymerization of methacrylate monomers bearing diacetylene moieties will suppress undesired side reactions—such as chain termination and transfer—by minimizing interactions between reactive methacrylate radicals and diacetylene groups, thereby enabling the synthesis of high-molecular-weight polymers.

Diacetylenes undergo topochemical polymerization in the solid state under UV irradiation to form π-conjugated polymers known as polydiacetylenes. Aliphatic polydiacetylenes, in particular, are known for forming highly conjugated, red-to-blue materials with exceptionally long effective conjugation lengths upon photopolymerization. Extensive studies have elucidated correlations between the molecular conformation of diacetylene units in the crystal lattice and the resultant degree of polymerization (DP).[25−29] Polydiacetylenes obtained via topochemical polymerization exhibit highly ordered molecular arrangements due to the single-crystal nature of their diacetylene monomers, resulting in desirable properties such as high charge carrier mobility,[30−34] pronounced third-order nonlinear optical (NLO) responses,[35−37] and superior mechanical strength and modulus.[38] However, 1,4-diphenylbuta-1,3-diyne derivatives typically fail to adopt conformations amenable to topochemical polymerization due to steric hindrance from the phenyl rings and their associated $\pi-\pi$ stacking interactions. As a result, these compounds often display poor or negligible photopolymerizability.[39−42] To address this challenge, various strategies have been devised to induce favorable conformations for topochemical polymerization via intermolecular interactions such as hydrogen bonding[43−47] and phenyl-fluorophenyl stacking.[37,48] Several approaches have also been developed to ensure a regular spatial arrangement of diacetylene units at defined intervals from the polymer backbone, thereby promoting extended conjugation lengths in the resulting polydiacetylenes. One approach involves using hydrogen bonding to attach side-chain 1,4-diphenylbuta-1,3-diyne mesogens to pendant groups on linear polymers, achieving periodic alignment relative to the main chain.[49] Another strategy employs reactive groups such as epoxides, which are tethered to diacetylene moieties via alkyl spacers; polymerization of the epoxide groups then ensures regular positioning of the diacetylene units.[50] These methods have successfully yielded polydiacetylenes with extended conjugation lengths, underscoring their potential in constructing highly ordered π-conjugated polymer systems. In the present work, we designed side-chain liquid crystalline polymers in which diacetylene moieties are arranged at regular intervals along a polymethacrylate backbone. This architecture is expected to facilitate confined polymerization in the solid state—such as in thin-film configurations—similar to the aforementioned systems.

We previously demonstrated the fabrication of thin films exhibiting highly ordered cylindrical microphase-separated structures using amphiphilic block copolymers composed of side-chain liquid crystalline polymers and hydrophilic poly(ethylene oxide) (PEO) segments.[51,52] Komura et al. showed that when such block copolymers are cast onto polyimide-coated substrates subjected to rubbing treatment, the PEO cylinder domains align uniaxially along the rubbing direction, producing striped nanostructures with ease.[53] The PEO domains, remaining fluid at ambient temperature, act as diffusion channels for metal ions[54−57] and small molecules.[58,59] In films where the cylinders are oriented perpendicular to the substrate, the domains span the film thickness and function as selective transport pathways, allowing passage of molecules ranging from small solutes to polymers of approximately 5 kDa.[60−62] Applying this methodology to side-chain liquid crystalline polymers containing diacetylene mesogens, we aimed to fabricate uniaxially aligned thin films and extend polydiacetylene chains along the alignment axis via UV irradiation. This strategy may yield an anisotropic electrical conductivity and enhanced NLO performance. Moreover, effective charge transport in conjugated polymers typically requires chemical doping. However, in topochemically polymerized polydiacetylenes, dopant diffusion is often hindered by crystallites, bulky side chains, and limited surface area.[63] By incorporation of PEO blocks into amphiphilic block copolymers containing diacetylene mesogens, the resulting PEO cylindrical domains can facilitate dopant diffusion—such as iodine—enabling uniform doping throughout the film, including the interior regions of the polydiacetylene domains. Furthermore, Oikawa et al. reported that multilayered structures consisting of uniaxially aligned polydiacetylene nanofibers and silver nanoparticles significantly enhance third-order NLO responses.[64] Building on our previous findings that silver ions can permeate PEO cylinder domains and be photoreduced to nanoparticles in azobenzene-containing block copolymer films, we anticipate that applying this strategy to microphase-separated films with directionally controlled poly(diacetylene) growth will further amplify their NLO properties.

EXPERIMENTAL SECTION

General. ^{1}H and ^{13}C NMR spectra were recorded using Bruker AVANCE II 300 and AVANCE III 600 spectrometers in $CDCl_3$. FTIR spectra were collected on a JASCO FT/IR-600 Plus spectrometer. Mass spectra were obtained on a JEOL JMS-700 instrument in FAB mode, using *m*-nitrobenzyl alcohol (NBA) as the matrix. Molecular weights of polymers were determined by gel permeation chromatography (GPC) using THF as the eluent with a TSK-gel HXL-M column (Tosoh). The chromatography system comprised a JASCO PU-2089 Plus HPLC pump, a Shimadzu CTO-20AC column oven (maintained at 40 °C), a JASCO UV-1570 UV detector, and a Shodex RI-101 refractive index detector. Number-average molecular weight (M_N) and weight-average molecular weight (M_W) were calculated using polystyrene standards (Shodex).

Thermal analyses were performed under a nitrogen atmosphere by using a Shimadzu DSC-60 system with a heating/cooling rate of ±10 °C/min. Polarized optical microscopy (POM) observations were carried out under an argon atmosphere using an Olympus BX53 microscope equipped with an Imoto IMC-0203 temperature control system. Temperature-dependent grazing-incidence X-ray scattering (GIXS) measurements were conducted at beamline 6A of the Photon Factory, High Energy Accelerator Research Organization (Tsukuba, Japan), using PILATUS-1 M and 100 K detectors. X-ray measurements were performed with a beam of wavelength 1.5 Å, and the incidence angle was set to 0.16°, near the critical angle of reflection for a silicon wafer, to optimize in-plane scattering signal detection.

https://doi.org/10.1021/acs.macromol.5c02107
Macromolecules XXXX, XXX, XXX−XXX

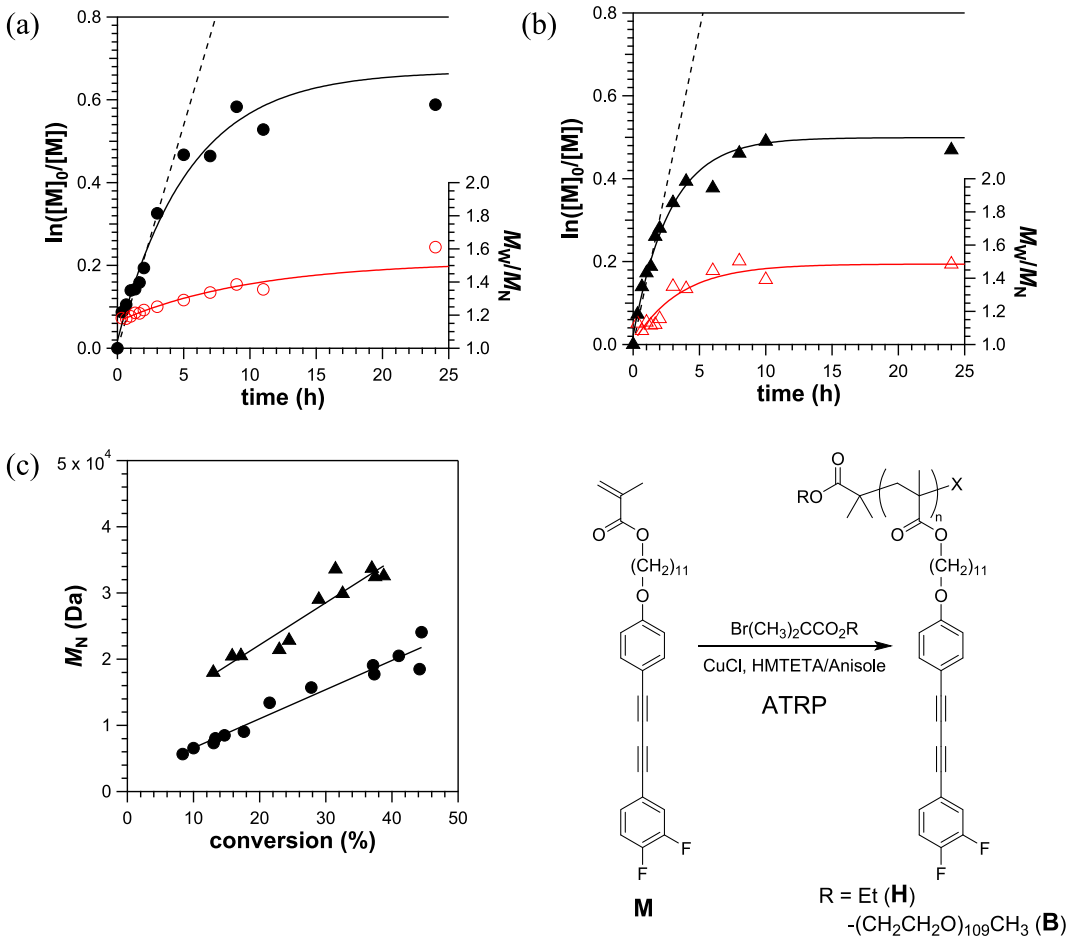

Figure 1. (a,b) Monomer concentration (closed symbols) and PDI (open symbols); (c) number-average molecular weight during the ATRP polymerization of monomer **M**, resulting in homopolymer **H** (circles) and block copolymer **B** (triangles).

Atomic force microscopy (AFM) was conducted using a Hitachi High-Tech Nanocute scanning probe microscope operated in tapping mode with silicon cantilevers (nano devices, nominal resonance frequency: 300 kHz). Samples were prepared by spin-coating 4.0 wt % toluene solutions of the block copolymers onto silicon wafers, glass substrates, or rubbed alignment films, followed by annealing at 130 °C for 5 h under vacuum. Transmission electron microscopy (TEM) images were acquired by using a JEOL JEM-2100 microscope operated at 200 kV. TEM samples were prepared by spin-coating polymer solutions onto glass substrates coated with fully hydrolyzed poly(vinyl alcohol) (PVA, average $M_W \approx 1000$, Wako). The resulting films were annealed at 130 °C for 5 h under vacuum, delaminated by dissolving the PVA layer in a 2-propanol/water mixture (1:4), and transferred onto copper grids. The films were then selectively stained by exposure to RuO_4 vapor for 2 min at room temperature to visualize the PEO domains.

Orientation films were fabricated by mechanically rubbing polyimide (PI) or PVA layers coated on silicon wafers or glass substrates by using an EHC MRJ-100 rubbing apparatus. The PI film was prepared as follows: equimolar amounts of 4,4′-biphthalic acid and 4,4′-diaminodiphenyl ether were dissolved in *N*-methylpyrrolidone (NMP) to form a polyamic acid solution, which was then diluted with a 1:1 mixture of NMP and γ-butyrolactone (GBL) to a concentration of 20 wt %. The resulting solution was spin-coated onto glass substrates and thermally imidized by baking at 150 °C for 1 h, followed by 250 °C for 2 h in air, yielding the PI alignment layer.

Materials. Dichloromethane was purified by fractional distillation over calcium hydride. Anisole and toluene were distilled over sodium/benzophenone under nitrogen. All other reagents were used as received from commercial sources. Monomer **M** was synthesized according to a modified procedure based on the report by Lu et al.,[16] as detailed in the Supporting Information. The macroinitiator α-methoxy-poly(ethylene oxide)-ω-(2-bromo-2-methylpropionate) (PEO-BMP) was prepared by esterification of poly(ethylene oxide) monomethyl ether (M_N = 4830, NOF) with 2-bromo-2-methylpropionyl bromide (TCI), following a previously reported method.

Polymerization. Homopolymers **H** were synthesized via ATRP following a standard protocol. A solution of Cu(I)Cl (6 mg, 60 μmol) and 1,1,4,7,10,10-hexamethyltriethylenetetramine (HMTETA, 18 μL, 66 μmol) in anisole (2 mL) was prepared, to which ethyl 2-bromo-2-methylpropionate (3 μL, 20 μmol) was added as an initiator. The mixture was stirred at 80 °C for 5 min under an argon atmosphere, followed by the addition of monomer **M** (1.0 g, 2.0 mmol), and the reaction was continued at 80 °C for 100 min. The resulting mixture was passed through a basic alumina column (Nacalai) using chloroform to remove the copper complex. After solvent evaporation, a ^{1}H NMR analysis was performed to determine the monomer conversion. The crude product was dissolved in a minimal amount of chloroform and precipitated into hexane to remove unreacted monomer. Reprecipitation from methanol yielded the homopolymer as a pale yellow powder (233 mg, 23% yield), which was used for characterization. Block copolymers **B** were synthesized by using the same procedure with PEO-BMP as the macroinitiator. The DP of the methacrylate segments was estimated from ^{1}H NMR spectra (see Supporting Information).

Photopolymerization of Thin Films. Thin films for photopolymerization were prepared by spin-coating 4.0 wt·% toluene solutions of **H** and **B** onto glass substrates or rubbed alignment layers, followed by annealing at 130 °C for 5 h under vacuum to obtain films with a thickness of approximately 150 nm. Photopolymerization of

https://doi.org/10.1021/acs.macromol.5c02107
Macromolecules XXXX, XXX, XXX−XXX

Table 1. Properties of Homopolymers (H) and Diblock Copolymers (B) Synthesized through ATRP[a]

	time (h)	conversion[b] (%)	M_N[c]	M_W/M_N[c]	DP[d]	LC content[f] (%)	tacticity[g] mm/mr/rr
$\mathbf{H}_{11k}$	1.67	26.1	11300	1.22	ND[e]	100	8/33/59
$\mathbf{H}_{23k}$	33	52.8	22800	1.43	ND[e]	100	7/33/60
$\mathbf{B}_{16k}$	1.67	30.8	16300	1.16	46.7	82.2	6/35/59
$\mathbf{B}_{30k}$	34	43.1	29900	1.47	54.8	84.4	6/34/60

[a]$[\mathbf{M}]_0$ = 1.0 M; polymerized in anisole under an argon atmosphere with a feed ratio of [initiator]/$[\mathbf{M}]_0$/[CuCl]/[HMTETA] = 1/100/3/3.3. [b]Conversions determined via ^{1}H NMR spectra. [c]Number-average molecular weight and polydispersity index determined through GPC analysis, based on polystyrene standards. [d]Degree of polymerization calculated from ^{1}H NMR spectra. [e]Not determined. [f]Weight fraction of the side-chain liquid-crystalline polymer segment based on DPs. [g]Tacticity of the triad in the polymethacrylate main chain determined from the corresponding peak area ratio of α-methyl protons in ^{1}H NMR spectra.

diacetylene units in **H** and **B** thin films was carried out using a SAN-EI Electric UVF-204S UV light source equipped with a HOYA U340 filter ($280 < \lambda < 380$ nm).

Computational Methods. Quantum chemical calculations were performed using the GAMESS software package.[65] Time-dependent density functional theory (TD-DFT) calculations were conducted by employing the B3LYP functional with the 6-31G* basis set. Excited-state energies and oscillator strengths were calculated to gain insight into the electronic transitions underlying the experimental observations.

RESULTS AND DISCUSSION

The radical polymerization of acrylates and methacrylates bearing diacetylene moieties in the ester side chains has been reported to be problematic due to the tendency of diacetylene units to trap propagating vinyl radicals.[13,15] Similarly, monomer **M**, in which a 1,4-diphenylbuta-1,3-diyne unit is incorporated via a long-chain alkyl ester linkage, was anticipated to exhibit limited polymerizability under radical conditions. Nevertheless, ATRP of **M**, initiated by ethyl 2-bromo-2-methylpropionate or a poly(ethylene oxide)-based macroinitiator (PEO-BMP) in the presence of a Cu(I)/HMTETA catalyst complex, successfully yielded the corresponding homopolymer (**H**) and block copolymer (**B**), respectively, with number-average molecular weights in the tens of kilodaltons. Under ATRP conditions, the propagating methacrylate radicals predominantly exist as dormant species rather than free radicals, thereby reducing the likelihood of radical trapping by the diacetylene units. Figure 1a,b presents the kinetic plots of $\ln([\mathbf{M}]_0/[\mathbf{M}])$ versus the polymerization time for **H** and **B**, respectively. In systems undergoing controlled/living radical polymerization, a linear relationship between $\ln([\mathbf{M}]_0/[\mathbf{M}])$ and time is expected, indicating first-order kinetics with respect to the monomer concentration. For **H**, linearity was observed up to 3 h, beyond which deviations were noted, with polymerization virtually ceasing after 10 h. A similar trend was observed for **B**, with linearity maintained up to 2 h and the reaction terminating after approximately 8 h. The PDI of the polymers remained below 1.3 in the early stages but increased with prolonged polymerization time. Figure 1c shows the relationship between the number-average molecular weight (M_N) and monomer conversion for **H** and **B**. In both cases, M_N increased linearly with conversion, suggesting that chain termination via radical recombination or transfer to the diacetylene moiety—potentially leading to cross-linking—was effectively suppressed under the ATRP conditions.

Representative properties of **H** and **B** obtained after 100 min and after more than 30 h of reaction are summarized in Table 1. The ^{1}H NMR spectra of **H** and **B** (Figure S1) exhibited three peaks in the 0.8−1.2 ppm region, assigned to the α-methyl groups on the polymethacrylate main chain. Triad tacticity ratios[66,67] calculated from these peaks confirmed that the polymers were completely atactic, as typically observed for ATRP-derived polymers. Importantly, the triad ratios remained unchanged over time, indicating a consistent polymerization mechanism throughout the reaction. The ^{13}C NMR spectra of **H** (Figure S2) showed four peaks between 72 and 83 ppm, attributable to the acetylenic carbon atoms. The absence of additional peaks, even after extended polymerization times, indicates that no significant structural changes or side reactions involving the diacetylene units occurred. Previous work by Burillo et al. suggested that methacrylate radicals can undergo intramolecular trapping by proximal diacetylene units in the side chains, leading to premature chain termination.[14] At high monomer concentrations during the initial stages of polymerization, the rate of propagation exceeds that of intramolecular trapping, favoring controlled polymerization. However, as the reaction proceeds and monomer concentration decreases, the influence of such termination reactions becomes more pronounced, contributing to broader molecular weight distributions. Consequently, $\mathbf{H}_{11k}$ and $\mathbf{B}_{16k}$—polymers obtained at earlier stages with minimal side reactions—were selected for further investigation.

The thermal behavior of $\mathbf{H}_{11k}$ and $\mathbf{B}_{16k}$ was characterized by differential scanning calorimetry (DSC), as shown in Figure 2. Upon the first cooling cycle of $\mathbf{H}_{11k}$, a broad exothermic event composed of multiple overlapping peaks was observed between 125 and 100 °C, accompanied by another broad peak centered at 41 °C. In the second heating scan, the corresponding broad endothermic peaks appeared at 45 °C and across the 105−135 °C range. $\mathbf{B}_{16k}$ exhibited similar thermal behavior. In the

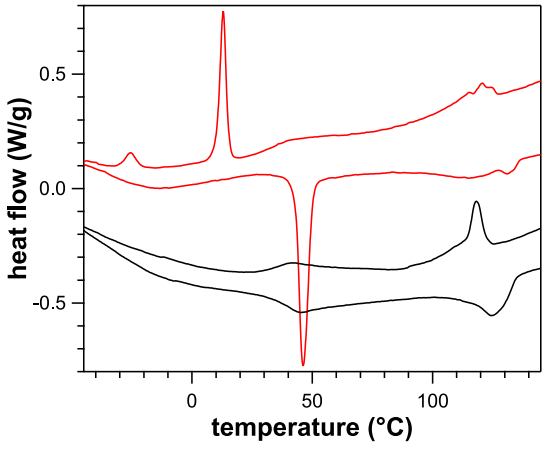

Figure 2. DSC profiles of $\mathbf{H}_{11k}$ (black lines) and $\mathbf{B}_{16k}$ (red lines) during the first cooling and second heating processes.

https://doi.org/10.1021/acs.macromol.5c02107
Macromolecules XXXX, XXX, XXX−XXX

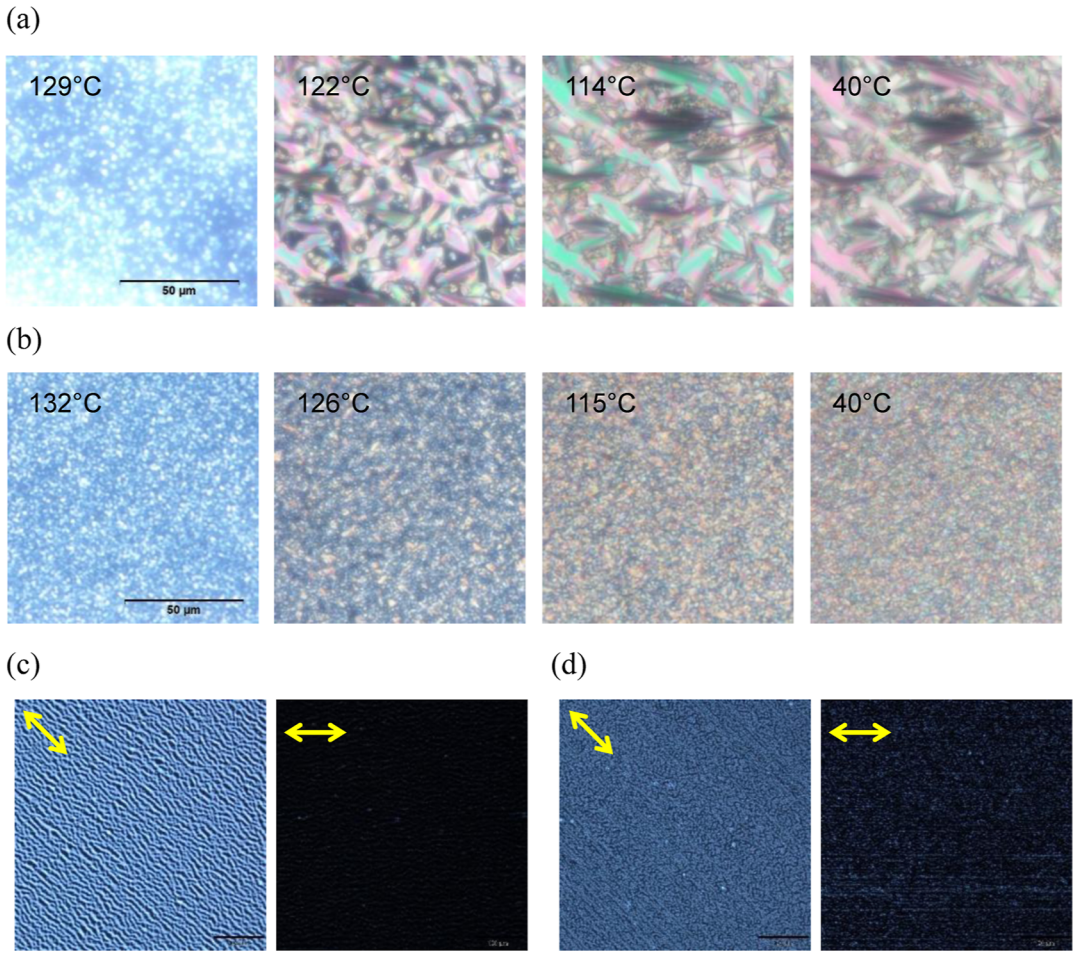

Figure 3. POM images of (a,b) thermally induced mesophase textures and (c,d) uniaxially aligned thin films of side-chain liquid crystalline polymers. (a,c) $\mathbf{H}_{11k}$; (b,d) $\mathbf{B}_{16k}$. In (c,d), images were taken with the rubbing direction oriented at 45° (left) and 0° (right) relative to the polarization direction of incident light under crossed polarizers. The arrows indicate the rubbing direction. Scale bars: 50 μm for (a,b); 100 μm for (c,d).

cooling scan, a broad exothermic transition with maxima at 115 °C, 121 °C, and 124 °C was detected below 127 °C, along with another exothermic peak at 42 °C. Upon heating, endothermic transitions with maxima at 116 °C, 131 °C, and 134 °C were observed above 100 °C, along with a sharp peak at 46 °C corresponding to the melting of the PEO segments. Additionally, a strong exothermic peak with a maximum at 12 °C appeared during cooling, and a minor peak at −26 °C was observed, which is significantly supercooled. This low-temperature event is attributed to the "confinement effect",[68] in which the minor PEO component is confined within nanoscale domains surrounded by the majority side-chain liquid crystalline polymer. These observations suggest the formation of a well-defined microphase-separated morphology.

POM observations under temperature-controlled conditions by using a hot stage were conducted to investigate the mesophase behavior of the synthesized polymers. For $\mathbf{H}_{11k}$, complete extinction was observed at temperatures above 130 °C, indicating the isotropic phase. Upon cooling below 129 °C, birefringence emerged, along with a grainy texture (Figure 3a). As the temperature dropped below 125 °C, domain growth became evident, and below 114 °C, a well-defined focal conic fan texture—characteristic of a smectic phase—was observed. Notably, this texture persisted from 103 °C down to room temperature, suggesting the formation of a stable smectic mesophase. These results indicate that $\mathbf{H}_{11k}$ exhibits a nematic phase between 129 and 125 °C and transitions to a smectic phase below 114 °C, confirming a thermotropic liquid crystalline behavior with a distinct phase transition. A similar mesophase sequence was observed for $\mathbf{B}_{16k}$, albeit with significantly smaller domain sizes (Figure 3b). Above 133 °C, the sample appeared dark, corresponding to the isotropic state. Below 132 °C, a granular texture emerged with slight domain growth observed below 127 °C. At 115 °C, minute focal conic textures were visible, indicating the onset of smectic ordering. Between 105 °C and room temperature, the texture remained largely unchanged, suggesting stabilization of the smectic structure at lower temperatures.

Drawing inspiration from the method developed by Komura et al., who achieved uniaxial alignment of side-chain liquid crystalline block copolymers bearing azobenzene mesogens via microphase separation,[53] we applied a similar approach to fabricate aligned thin films. Solutions of $\mathbf{H}_{11k}$ and $\mathbf{B}_{16k}$ in toluene were spin-coated onto polyimide-coated glass substrates, serving as alignment layers. Unlike Komura's method, no polydimethylsiloxane (PDMS) overlay was applied in our protocol. The films were then thermally annealed at 130 °C, near the isotropic transition temperature, for 5 h and subsequently examined by POM. In both $\mathbf{H}_{11k}$ and $\mathbf{B}_{16k}$ films, having the thickness of 130 and 170 nm, respectively,

https://doi.org/10.1021/acs.macromol.5c02107
Macromolecules XXXX, XXX, XXX−XXX

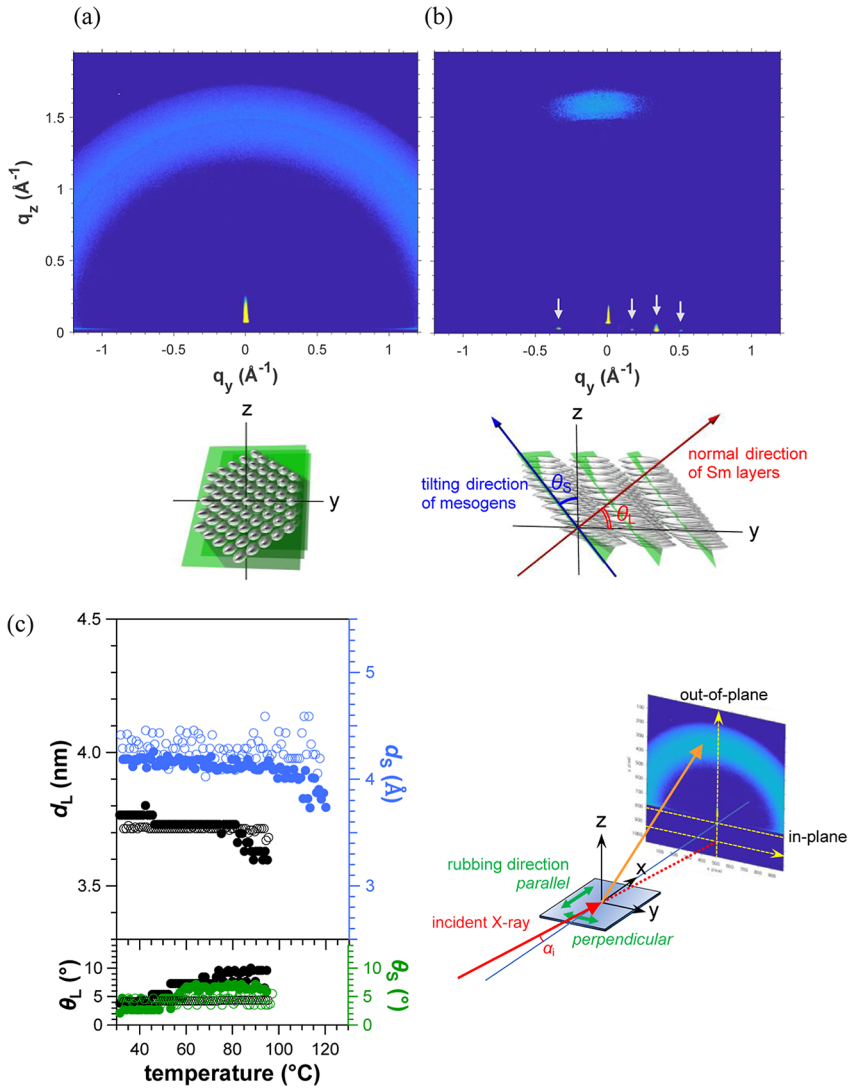

Figure 4. GI-WAXS patterns of the $\mathbf{H}_{11k}$ thin film fabricated on the alignment layer: X-ray incidence at (a) parallel and (b) perpendicular to the rubbing direction. The arrows in (b) indicate the positions of the scattering peaks observed on the Yoneda wing. The corresponding schematic illustrations of the assumed molecular arrangements are shown below each 2D scattering profile. (c) Temperature dependence of the layer spacing (d_L), mesogen stacking distance (d_S), and tilt angles (θ_L and θ_S) calculated from the scattering peaks: $\mathbf{H}_{11k}$ (closed circles); $\mathbf{B}_{16k}$ (open circles).

the POM images exhibited characteristic birefringence patterns: the films appeared darkest when the rubbing direction was parallel (0°) to the polarization direction of incident light and brightest at 45°, indicating uniaxial alignment of the liquid crystalline mesogens (Figure 3c,d). The birefringence (Δn), calculated from the optical retardation of the films, was determined to be 0.58 for $\mathbf{H}_{11k}$ and 0.22 for $\mathbf{B}_{16k}$. For comparison, a structurally related low-molecular-weight liquid crystal containing a 1-(3,4-difluorophenyl)-4-phenylbuta-1,3-diyne core exhibits a Δn of 0.264,[69] while a side-chain polymethacrylate bearing 1,4-diphenylbuta-1,3-diyne mesogens synthesized via anionic polymerization has a reported Δn of 0.41.[12] These findings indicate that $\mathbf{H}_{11k}$ possesses exceptionally high birefringence, surpassing or comparable to those of these benchmark systems.

The thin film of $\mathbf{H}_{11k}$ was fabricated by using a silicon substrate treated with a polyimide alignment layer, and its structural characteristics were investigated via grazing-incidence wide-angle X-ray scattering (GI-WAXS). The incident X-ray beam was directed either parallel or perpendicular to the rubbing direction of the alignment layer, and the resulting 2D scattering patterns are presented in Figure 4a,b, respectively. Figure 4a displays a broad halo centered at $q \approx 1.5$ Å^{-1}, where q is the magnitude of the scattering vector defined as $q = (4\pi/\lambda_X)\sin(\theta/2)$, with θ being the scattering angle and λ_X the X-ray wavelength. This feature is attributed to the lateral stacking of mesogenic units aligned along the rubbing direction, and its breadth indicates a lack of long-range order. The peak position corresponds to an average termesogen distance of 4.2 Å. In contrast, Figure 4b exhibits discrete diffraction spots along the horizontal Yoneda wing at $q_y = 0.17$, 0.33, and 0.50 Å^{-1}, where q_y is the magnitude of in-plane scattering vector component along the direction parallel to the sample surface and perpendicular to the incident beam. The nearly uniform spacing between these spots indicates the presence of a lamellar structure with an interlayer spacing of 3.76 nm. Additionally, weak vertical scattering at $q_z \approx 1.5$ Å^{-1}, where q_z is the magnitude of the out-of-plane scattering vector component perpendicular to the sample surface, consistent with the halo in Figure 5a, suggests perpendicularly oriented

https://doi.org/10.1021/acs.macromol.5c02107
Macromolecules XXXX, XXX, XXX−XXX

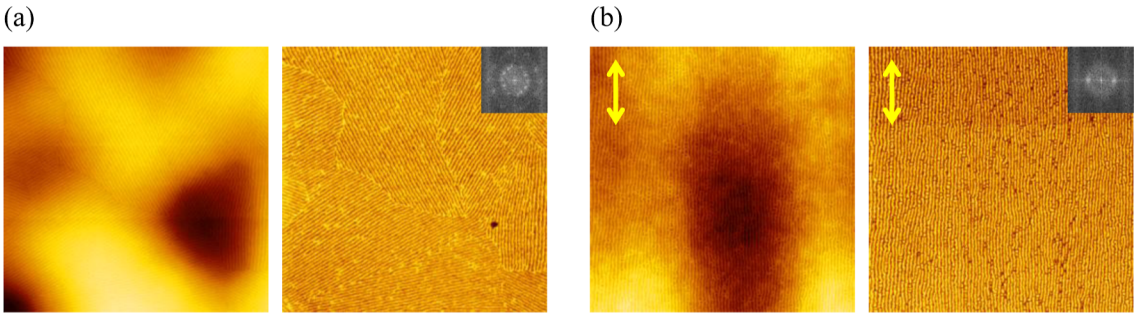

Figure 5. AFM images (2 μm × 2 μm) of the $\mathbf{B}_{16k}$ thin film surface fabricated on (a) a silicon wafer and (b) an alignment layer: (left) height images; (right) phase-shift images. The arrows indicate the rubbing direction. The inset in each phase-shift image shows the full FFT pattern.

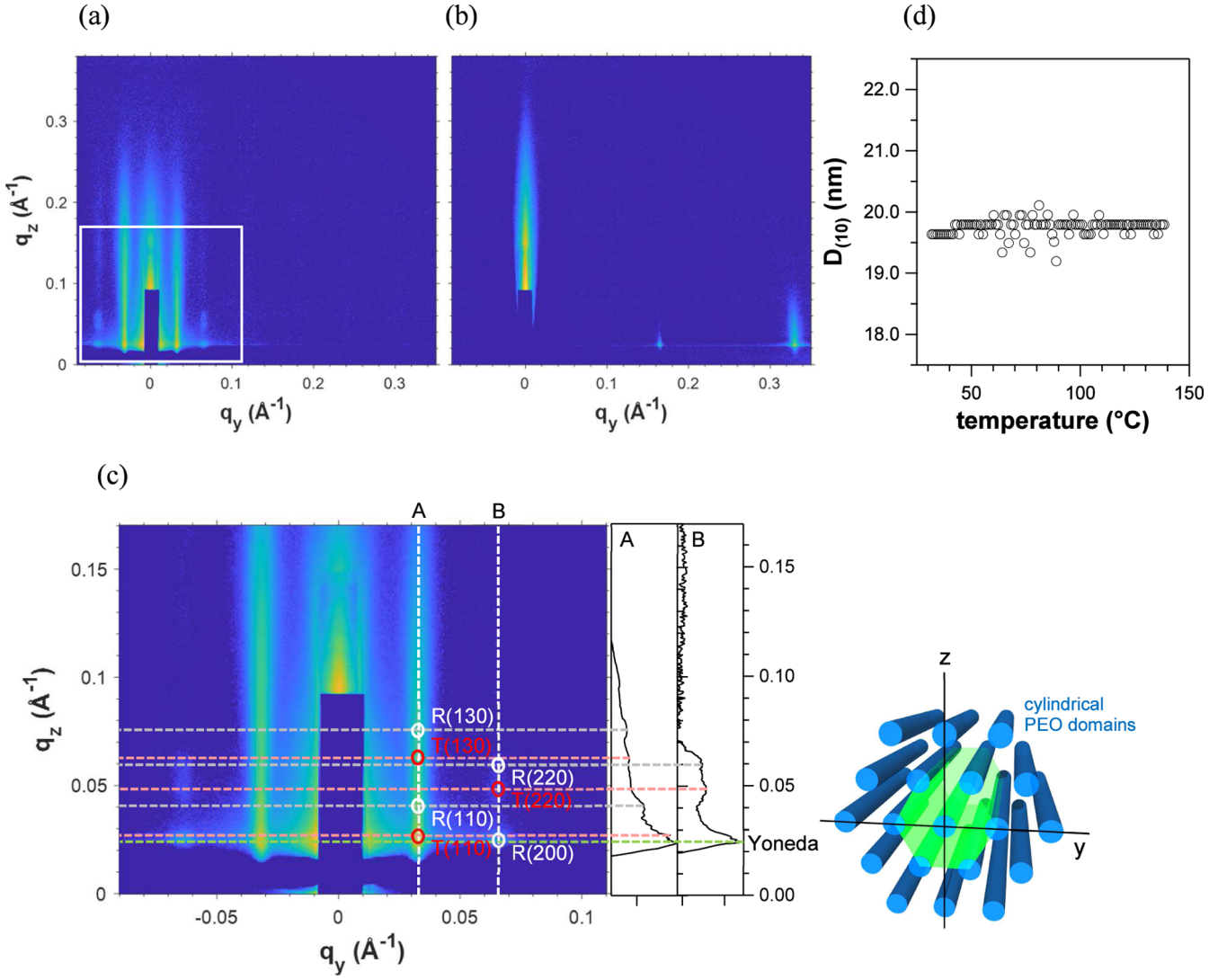

Figure 6. GI-SAXS patterns of the $\mathbf{B}_{16k}$ thin film fabricated on the alignment layer with X-ray incidence (a) parallel and (b) perpendicular to the rubbing direction. (c) Enlarged view of the white square region in (a), showing scattering from both transmitted (T) and reflected (R) X-rays with assigned Miller indices. The schematic on the right depicts the proposed hexagonally packed cylindrical microphase-separated structure. The [010] crystallographic direction is oriented perpendicular to the substrate. (d) Temperature dependence of the interplanar spacing $D(10)$ corresponding to the (10) plane of the cylindrical domains.

smectic layers relative to the substrate. Defining θ_L as the azimuthal angle of the second-order lamellar diffraction peak (the most intense among the horizontal reflections) and θ_S as the angle between the vertical axis and the weak vertical scattering (corresponding to mesogen stacking), both angles can be interpreted as measures of the mesogen tilt with respect to the smectic layer normal. However, due to geometric constraints inherent to GI-WAXS, reflections with q_y below the Yoneda wing are unobservable, leading to potential inaccuracies in determining θ_L, especially at small azimuthal angles.

https://doi.org/10.1021/acs.macromol.5c02107
Macromolecules XXXX, XXX, XXX−XXX

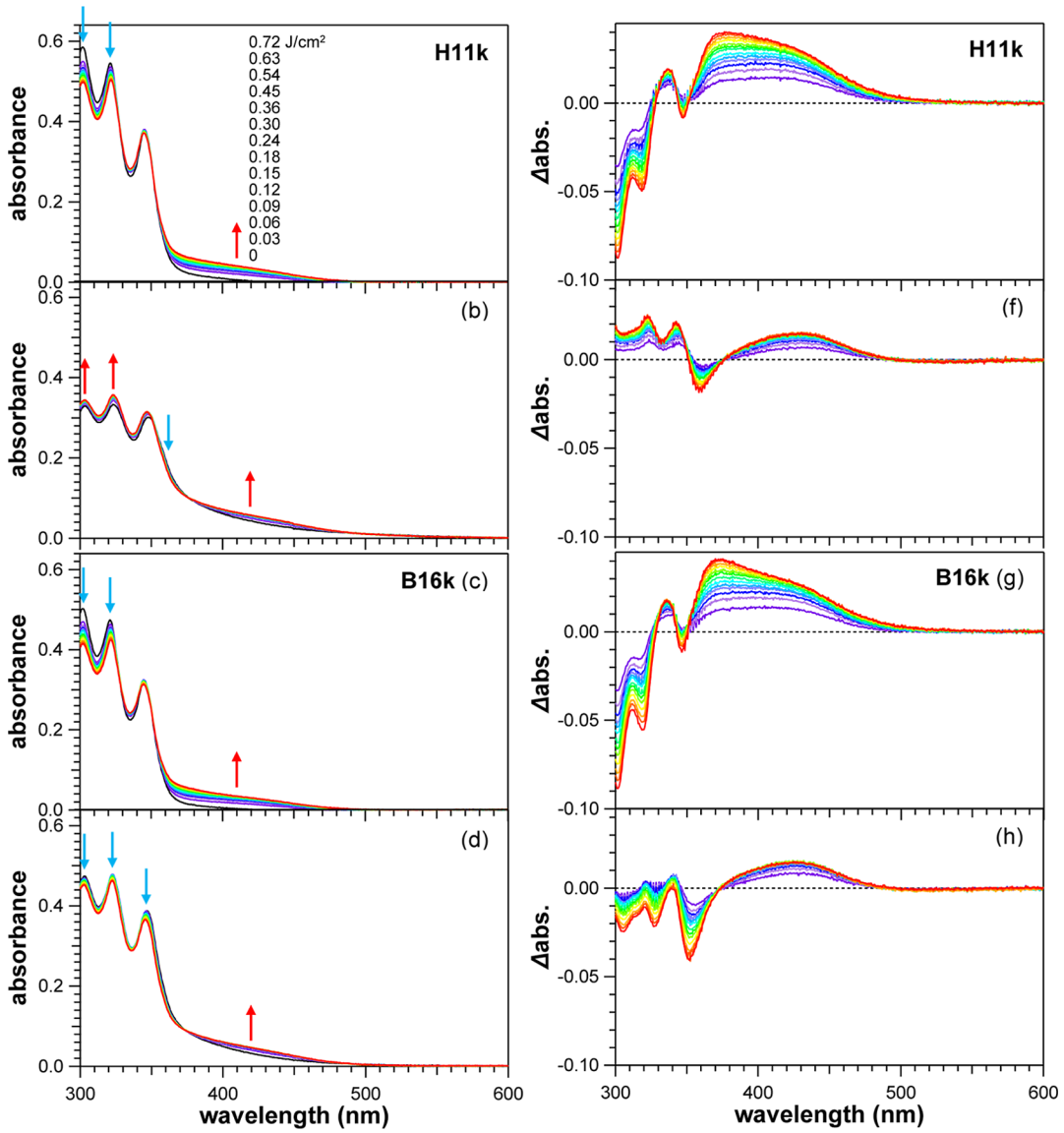

Figure 7. UV−vis absorption spectra of side-chain liquid crystalline polymer thin films on glass substrates under photoirradiation ($280 < \lambda < 380$ nm, 3 mW/cm^2). (a,b) Absorption spectra of **H11k**; (c,d) absorption spectra of **B16k**. Pristine films are shown in (a,c), and annealed films in (b,d). (e−h) Differential spectra corresponding to (a−d), calculated relative to the spectra before photoirradiation.

Therefore, θ_S was also evaluated as a complementary parameter. The measured tilt angles were $\theta_L = 3.8°$ and $\theta_S = 2.1°$, indicating a smectic A (SmA) phase characterized by a minimal molecular tilt.

To investigate the thermally induced structural evolution of the liquid crystalline phase within the thin film, a sample was fabricated by spin-coating a 10 wt % PDMS solution in hexane onto the $\mathbf{H}_{11k}$ film surface, thereby creating a PDMS-modified air interface. The sample was then subjected to in situ heating under a nitrogen atmosphere, and changes in the scattering profiles were monitored accordingly. The horizontal diffraction spots observed under perpendicular X-ray incidence persisted up to 95 °C but disappeared at higher temperatures. The halo under parallel incidence was detectable up to approximately 120 °C, beyond which the scattering intensity markedly decreased. Figure 4c illustrates the temperature dependence of the smectic layer spacing (d_L), in-layer mesogen distance (d_S), and tilt angles (θ_L and θ_S), derived from the scattering profiles. The d_L value remained nearly constant up to ∼80 °C and then exhibited a slight decrease between 80 and 95 °C. Although the tilt angle slightly increased with temperature, it remained below 9.6° throughout, consistent with a thermally stable SmA phase. The d_S value was nearly constant below 95 °C and slightly decreased at elevated temperatures. Despite the absence of well-defined lamellar reflections above 95 °C, POM revealed focal conic fan textures, suggesting the persistence of a weakly ordered smectic phase with characteristics intermediate between SmA and nematic phases, likely due to partial disruption of the layer structure.

A uniaxially aligned thin film of $\mathbf{B}_{16k}$ was also prepared and examined via GI-WAXS. The scattering profiles obtained under both parallel and perpendicular incidence were analogous to those observed for $\mathbf{H}_{11k}$ (Figure S3). Upon PDMS surface coating and thermal treatment, the diffraction spots observed under perpendicular incidence disappeared at 95 °C, similar to $\mathbf{H}_{11k}$. However, the peak positions remained virtually unchanged, and the layer spacing d_L, calculated from the diffraction peaks, was approximately 3.7 nm and remained

https://doi.org/10.1021/acs.macromol.5c02107
Macromolecules XXXX, XXX, XXX−XXX

stable with a tilt angle of less than 4.4°. Similarly, the halo observed under parallel incidence exhibited a negligible shift in peak position from room temperature to ∼120 °C. These observations suggest that the formation of microphase-separated structures in $\mathbf{B}_{16k}$ thin films significantly suppresses the structural transitions typically observed in liquid crystalline phases, likely due to the reduced molecular mobility associated with the segregated domains.

To further investigate the microphase-separated morphology of $\mathbf{B}_{16k}$, a thin film was prepared on a silicon substrate, and its surface structure was examined by AFM. As shown in Figure 5a, the film exhibited numerous striped domains, several μm^2 in size, with varying orientations. According to the report by Komura et al.,[53] amphiphilic liquid-crystalline block copolymers incorporating azobenzene as a mesogenic unit exhibit a vertically oriented cylindrical microphase-separated structure in thin films relative to the substrate, thereby requiring a PDMS overlay to induce horizontal orientation. In contrast, our thin films exhibit preferential horizontal alignment, even without a PDMS overlay. The surface of a $\mathbf{B}_{16k}$ film spin-coated onto a silicon substrate with a polyimide alignment layer exhibited highly ordered, linearly aligned structures across the entire surface. These structures were strictly parallel to the rubbing direction and showed a uniform periodicity of 24.4 ± 0.9 nm (Figure 5b).

To probe the internal morphology of the aligned $\mathbf{B}_{16k}$ film, we performed grazing-incidence small-angle X-ray scattering (GI-SAXS) measurements. The scattering profiles with the X-ray beam incident parallel and perpendicular to the rubbing direction are shown in Figure 6a,b, respectively. Figure 6b displays first- and second-order reflections originating from smectic layering, aligned along the Yoneda wing, consistent with the GI-WAXS results. No distinct features were detected in the low-q region. In contrast, Figure 6a reveals multiple sharp scattering spots at q_y = 0.032 and 0.064 $Å^{-1}$. As shown in the magnified low-q region (Figure 6c), the positions of these reflections correspond to a hexagonally packed cylindrical morphology. This indicates the formation of a uniaxially aligned hexagonal-cylinder-type microphase-separated structure, oriented parallel to the rubbing direction. From the q_y values, the interplanar spacing of the (10) plane perpendicular to the substrate was calculated to be $D(10)$ = 19.6 nm.

To investigate the thermal stability of this morphology, a PDMS-coated $\mathbf{B}_{16k}$ film was subjected to in situ GI-SAXS measurements during heating under nitrogen. Above 60 °C, although the q_y positions of the scattering peaks at 0.032 and 0.064 $Å^{-1}$ remained largely unchanged, the initially discrete spots along the q_z direction became diffuse, forming a continuous scattering streak along the z-axis. Upon reaching the isotropic transition temperature, the scattering pattern transformed into one characteristic of a body-centered tetragonal structure (Figure S2). Similar thermal behavior has been reported in amphiphilic liquid crystalline block copolymers bearing azobenzene mesogens, in which vertically aligned hexagonal cylinder structures undergo transformation into body-centered cubic[70] or face-centered orthorhombic[71] structures upon heating. These results suggest that $\mathbf{B}_{16k}$ undergoes a comparable order−order transition from a hexagonally packed cylindrical morphology to a BCT-like structure near the isotropic transition.

A thin film of $\mathbf{B}_{16k}$ was deposited onto a CaF_2 substrate and irradiated with ultraviolet light through a U340 filter ($280 < \lambda < 380$ nm), while monitoring changes in the infrared absorption spectrum (Figure S5). Peaks observed at 2215 and 2146 cm^{-1} prior to irradiation, attributed to carbon−carbon triple bonds, gradually decreased in intensity with prolonged exposure. Simultaneously, a broad absorption band centered at around 2185 cm^{-1} became increasingly prominent. This spectral evolution indicates a photochemical rearrangement of the triple bonds and the formation of newly configured carbon−carbon triple bonds during the reaction. Analogous UV irradiation experiments were conducted on $\mathbf{H}_{11k}$ thin films fabricated on glass substrates, both in the pristine state and after thermal annealing. The corresponding changes in the UV−vis absorption spectra are shown in Figure 7a,b. Upon irradiation, a broad absorption band extending to approximately 500 nm emerged on the longer-wavelength side of the mesogen-associated bands, which exhibit maxima at 303, 322, and 346 nm. The intensity of this broad band increased with accumulated UV dose. Difference spectra before and after irradiation are presented in Figure 7e,f. In the pristine film, the most pronounced increase in absorbance was observed around 380 nm, whereas in the annealed film, the most significant enhancement appeared near 430 nm. Comparable trends were observed in $\mathbf{B}_{16k}$ films, where the annealed samples exhibited more substantial spectral changes at longer wavelengths than their pristine counterparts (Figure 7c,d; difference spectra in Figure 7g,h). It is well established that diacetylenes undergo 1,4-addition photopolymerization upon UV irradiation. Depending on their relative orientation, either head-to-tail or head-to-head addition is favored (Chart 1).[26,29,45,72] For aliphatic diacetylenes, *trans*-polydiacetylenes are predominantly formed via head-to-tail addition when the center-to-center distance between diacetylene units is 4.7−5.2 Å and the molecular axis is inclined at approximately 45° relative to the stacking axis. Conversely, when the intercenter distance is 3.4−3.6 Å and the angle is 90°, head-to-head addition yields *cis*-polydiacetylenes with high efficiency. X-ray diffraction (XRD) profiles of drop-cast films of $\mathbf{H}_{11k}$ and $\mathbf{B}_{16k}$ on silicon substrates (Figure S6) revealed that in the annealed films, a peak at q = 0.34 $Å^{-1}$, attributable to a smectic lamellar structure, was observed in the low-q region. In contrast, pristine films exhibited multiple peaks at different q values (q = 0.25 and 0.38 $Å^{-1}$ for $\mathbf{H}_{11k}$; q = 0.24 and 0.36 $Å^{-1}$ for $\mathbf{B}_{16k}$), indicating the coexistence of domains with different layer spacings. In addition, although the annealed films showed a broad peak centered around q = 1.5 $Å^{-1}$ in the wide-angle region, assigned to mesogen stacking, the pristine films exhibited multiple distinct peaks, suggesting the presence of domains with different stacking distances between mesogens. Although the tilt angle could not be determined, the peak near q = 1.3 $Å^{-1}$ corresponds to the intermolecular distance favorable for head-to-tail addition, while that near q = 1.9 $Å^{-1}$ is closer to that favorable for head-to-head addition. Thus, the higher photoreaction rate observed in pristine films compared to that in annealed films can be attributed to these structural features. To investigate the electronic properties of the resulting materials, TD-DFT (B3LYP/6-31G*) calculations were performed on both *trans* and *cis* oligomeric models derived from 1-(3,4-difluorophenyl)-4-(4-methoxyphenyl)buta-1,3-diyne as a representative monomer. As the π-conjugation length increased from dimer to tetramer models, the lowest-energy absorption band corresponding to the HOMO−LUMO transition exhibited a pronounced red-shift, moving from 350 nm to the 540−580 nm region (Figure S7). In pristine films, although conformations favorable for photopolymerization are partially

https://doi.org/10.1021/acs.macromol.5c02107
Macromolecules XXXX, XXX, XXX−XXX

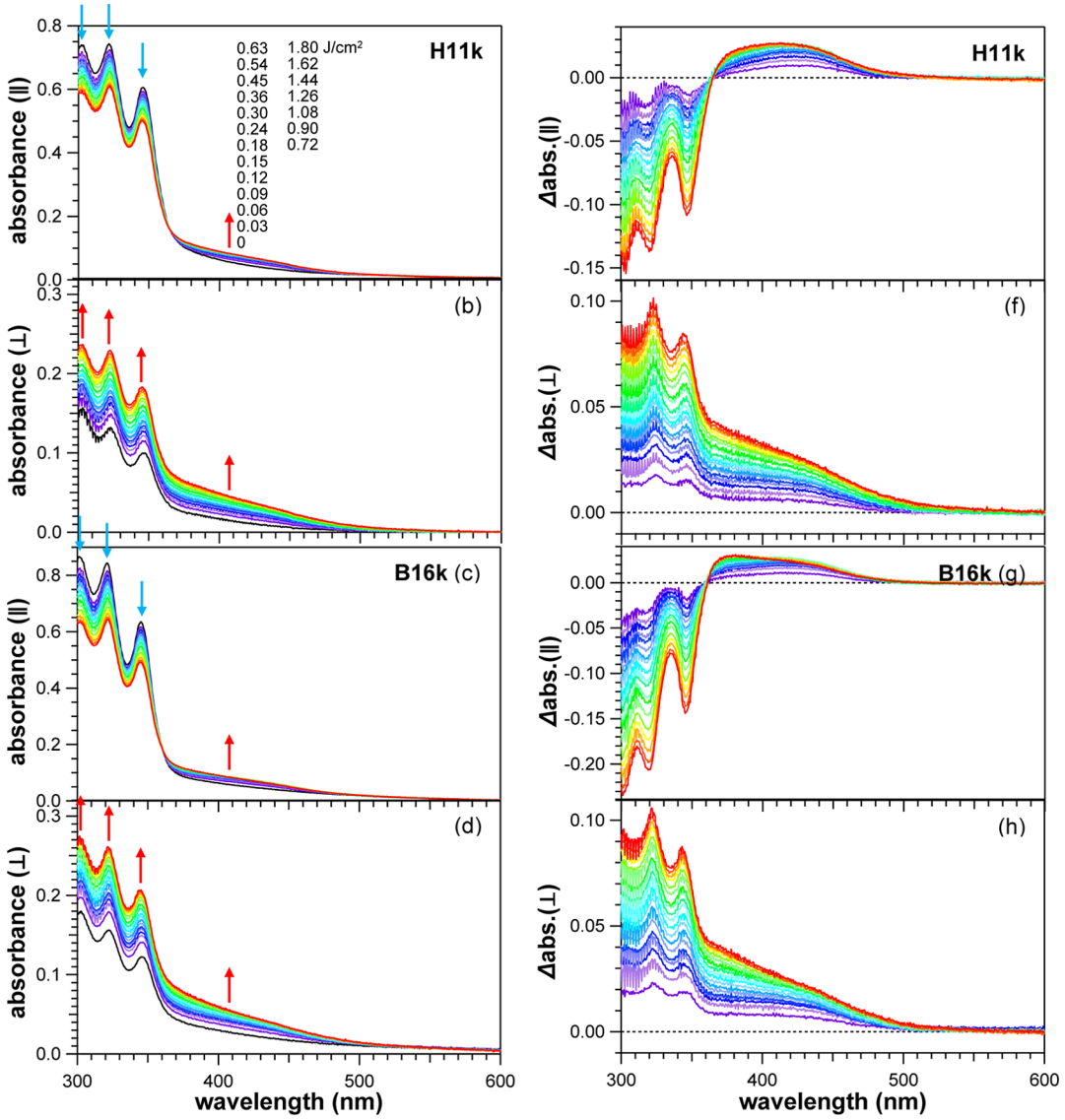

Figure 8. Polarization-dependent absorption spectra of side-chain liquid crystal polymer thin films on polyimide alignment films coated glass substrates upon photoirradiation ($280 < \lambda < 380$ nm, 3 mW/cm^2): absorption spectra of **H11k** (a,b) and **B16k** (c,d) measured with light polarized parallel (a,c) or normal (b,d) to the rubbing direction; (e−h) differential spectra of (a−d), calculated with respect to the spectra before photoirradiation.

present, the coexistence of multiple conformational states leads to poor long-range structural order. Consequently, the products are mostly short oligomers with short conjugation lengths. In contrast, annealed films lack the optimal intermolecular distances for either head-to-tail or head-to-head addition, resulting in slower reaction rates. However, their higher uniformity and long-range order allow for more extensive polymerization, giving polymers with relatively longer conjugation lengths. The simulated spectra further revealed that, for each DP, the *trans* isomers exhibit more significant red-shifts in the lowest-energy absorption bands compared to their *cis* counterparts. This is attributable to structural differences: the carbon backbone of the *trans* oligomers adopts an almost planar configuration, allowing for extended π-conjugation, whereas the *cis* oligomers suffer from steric hindrance between aromatic rings at the head−head and tail−tail positions. This torsional strain disrupts the planarity and limits conjugation. As noted above, GI-SAXS analyses of the $\mathbf{H}_{11k}$ and $\mathbf{B}_{16k}$ films indicate that while neither the head-to-tail nor head-to-head arrangement is ideally satisfied, the molecular packing appears to be somewhat more favorable for head-to-head addition. Langmuir−Blodgett (LB) films of linear aliphatic diacetylenes—where molecules are highly ordered in a layered arrangement—have demonstrated that ideal head-to-tail alignment yields polydiacetylenes with exceptionally long effective conjugation lengths, characterized by a strong absorption maximum near 640 nm.[73−78] However, thermal annealing can disrupt this molecular ordering, leading to shortened conjugation lengths and a hypsochromic shift of the absorption maximum to approximately 530 nm. In the $\mathbf{H}_{11k}$ and $\mathbf{B}_{16k}$ films examined here, the predominance of twisted backbones resulting from head-to-head addition appears to restrict effective conjugation lengths, thereby confining the absorption edge to approximately 500 nm.

Uniaxially aligned thin films of $\mathbf{H}_{11k}$ and $\mathbf{B}_{16k}$ were fabricated on glass substrates coated with polyimide alignment layers. These films were irradiated at normal incidence with linearly polarized UV light with polarization oriented parallel or

https://doi.org/10.1021/acs.macromol.5c02107
Macromolecules XXXX, XXX, XXX−XXX

perpendicular to the rubbing direction, and the resulting polarized absorption spectra were recorded (Figure 8). The dichroic ratio at 346 nm, defined as $R = A_{\parallel}/A_{\perp}$, was 6.1 for $\mathbf{H}_{11k}$ and 5.2 for $\mathbf{B}_{16k}$, corresponding to order parameters $S = (R - 1)/(R + 1)$ of 0.63 and 0.58, respectively. During UV irradiation, the polarized spectra were monitored over time. Under parallel polarization for $\mathbf{H}_{11k}$ (Figure 8a), the absorbance peaks at 303, 322, and 346 nm, attributed to mesogen absorption, gradually diminished, while a broad band emerging beyond 365 nm and extending to ~500 nm increased in intensity. In contrast, the perpendicular polarization spectrum (Figure 8b) exhibited a monotonic increase in the absorbance across 300−550 nm. Similar spectral evolutions were observed for $\mathbf{B}_{16k}$ (Figure 8c,d). Maximum absorption occurs when the incident light polarization aligns with the chromophore's transition dipole moment. TD-DFT simulations of 1-(3,4-difluorophenyl)-4-(4-methoxyphenyl)buta-1,3-diyne (Figure S6a) assign the bands near 320 and 350 nm to dipoles along the molecular long axis. Because the mesogens align parallel to the rubbing direction, these bands are preferentially consumed during photopolymerization, producing a more pronounced decrease in absorbance for parallel-polarized light (Figure 8e,g). The polydiacetylene backbone elongation direction in both *cis* and *trans* oligomers was calculated to be ~80° relative to the mean side-chain direction, coinciding with the HOMO−LUMO transition dipole responsible for the longest-wavelength absorption (Figure S6b−g). Figure 9 plots the red-edge wavelength of each

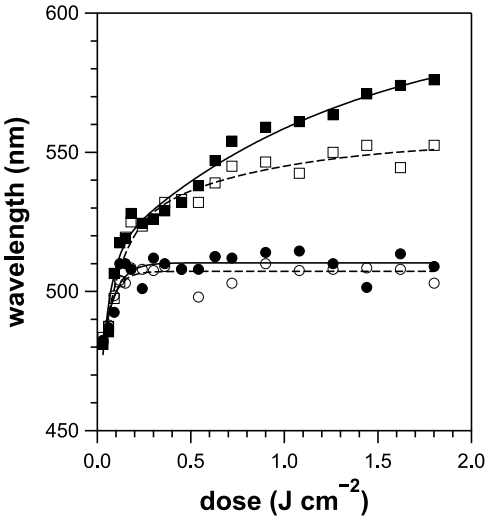

Figure 9. Absorption edge wavelength of the thin film as a function of the ultraviolet irradiation dose per unit area, obtained from the absorption spectra for light polarized parallel (circles) and perpendicular (squares) to the rubbing direction. $\mathbf{H}_{11k}$ (filled symbols) and $\mathbf{B}_{16k}$ (open symbols).

absorption spectrum versus the incident UV dose per unit area, derived from Figure 8e−h. Under parallel polarization, the red edge for both $\mathbf{H}_{11k}$ and $\mathbf{B}_{16k}$ initially red-shifted by ~30 nm before plateauing, whereas under perpendicular polarization, it continued to red-shift throughout irradiation by >90 nm for $\mathbf{H}_{11k}$ and >60 nm for $\mathbf{B}_{16k}$. These results indicate that polydiacetylene backbones preferentially elongate perpendicular to the rubbing direction, with $\mathbf{H}_{11k}$ forming higher-molecular-weight polymers exhibiting longer effective conjugation lengths than $\mathbf{B}_{16k}$. Meanwhile, the birefringence (Δn) of $\mathbf{H}_{11k}$ and $\mathbf{B}_{16k}$ films gradually decreased upon photoirradiation, reaching values of 0.38 and 0.11 at 1.8 J/cm^2 dose, respectively.

Chart 1. Molecular Structures of Polydiacetylene Generated by Photopolymerization of Diphenyldiacetylene Mesogenic Units in the Side Chains

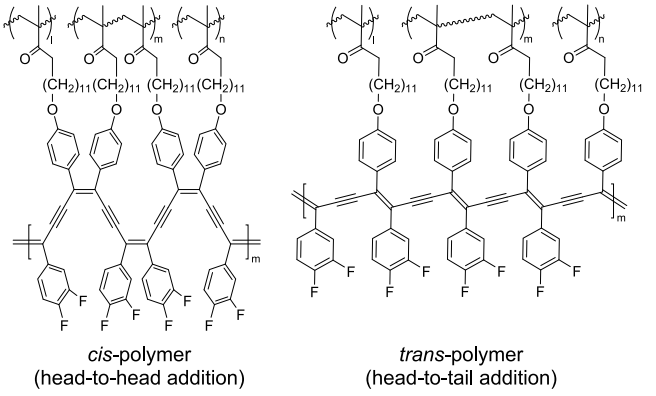

A microphase-separated thin film of $\mathbf{B}_{16k}$ was fabricated on a silicon substrate coated with a rubbed poly(vinyl alcohol) (PVA) alignment layer. Following UV irradiation to induce polymerization of the diacetylene moieties, the film was immersed in a 2-propanol/water mixture (1:4 v/v) to dissolve the PVA layer, thereby enabling delamination of the film for structural analysis. TEM was then performed on the resulting free-standing film (Figure 10b). For comparison, a $\mathbf{B}_{16k}$ thin

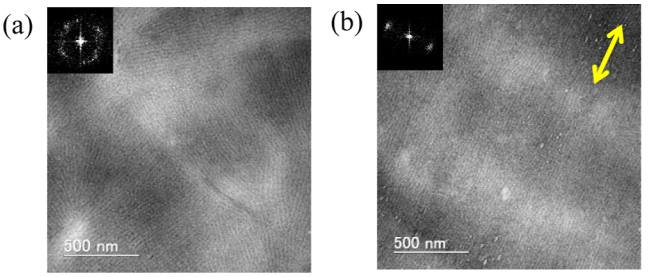

Figure 10. TEM images of $\mathbf{B}_{16k}$ thin films fabricated on (a) an unrubbed and (b) a rubbed PVA layer. The PEO domains were selectively stained with RuO_4 vapor. The arrow indicates the rubbing direction. The inset in each image shows the full FFT pattern.

film was also prepared on an unrubbed PVA layer, with the corresponding TEM image shown in Figure 10a. In the film prepared on the unrubbed PVA layer (Figure 10a), multiple stripe-like domains with varying orientations were observed, each spanning several square micrometers and exhibiting periodic spacings in the range of 21−25 nm. In contrast, the film on the rubbed PVA substrate (Figure 10b) exhibited a uniaxially aligned stripe-like morphology with a uniform spacing of approximately 21.5 nm, oriented parallel to the initial rubbing direction. These TEM results were evaluated alongside AFM images acquired prior to UV exposure (Figure 5a,b), as well as with the cylinder-to-cylinder distances determined from GI-SAXS. Although minor variations in intercylinder spacing were detected following UV irradiation, the overall hexagonally packed cylindrical morphology was well retained. These findings strongly support the idea that the photopolymerization of the diacetylene units proceeded via a

https://doi.org/10.1021/acs.macromol.5c02107
Macromolecules XXXX, XXX, XXX−XXX

topochemical mechanism, enabling the formation of covalent polymer backbones with minimal disruption to the nanostructural order.

CONCLUSION

In this study, we successfully synthesized side-chain liquid crystalline polymers incorporating 1,4-diphenylbuta-1,3-diyne moieties via ATRP, overcoming challenges associated with the radical-trapping nature of diacetylene units and achieving precise control over the polymer architecture. POM and UV−vis absorption spectroscopy confirmed the formation of highly ordered, uniaxially aligned liquid crystalline thin films. Upon UV irradiation, the observed changes in polarized absorbance revealed that the poly(diacetylene) backbones preferentially grew perpendicular to the rubbing direction. The progressive red-shift of the absorption edge, particularly for light polarized perpendicular to the alignment direction, indicates the formation of high-molecular-weight polymers with extended conjugation lengths. GIXS provided insight into the intricate nanostructural organization, revealing features such as lamellar stacking and microphase-separated cylindrical domains. Complementary TEM analysis confirmed that UV-induced polymerization proceeded through a topochemical pathway, preserving the underlying hexagonally packed morphology. These results collectively demonstrate the feasibility of constructing hierarchically ordered, π-conjugated polymeric materials through the integration of liquid crystalline alignment and confined polymerization strategies.

ASSOCIATED CONTENT

Supporting Information

The Supporting Information is available free of charge at https://pubs.acs.org/doi/10.1021/acs.macromol.5c02107.

Synthetic procedures for the monomer, macroinitiator, and polymers and additional figures, including GI-WAXS profiles of polymer thin films measured at ambient temperature, GI-SAXS profiles obtained above the isotropic transition temperature, FTIR spectral changes upon photoirradiation, XRD profiles of drop-cast polymer films, and simulated absorption spectra of model oligomers calculated by TD-DFT (PDF)

AUTHOR INFORMATION

Corresponding Author

Sadayuki Asaoka − *Faculty of Materials Science and Engineering, Kyoto Institute of Technology, Sakyo-ku, Kyoto 606-8585, Japan; Division of Integrated Molecular Engineering, Chemical Resources Laboratory, Tokyo Institute of Technology, Yokohama, Kanagawa 226-8503, Japan;* orcid.org/0009-0005-1456-7942; Email: sada@kit.ac.jp

Authors

Satoru Tamaki − *Division of Integrated Molecular Engineering, Chemical Resources Laboratory, Tokyo Institute of Technology, Yokohama, Kanagawa 226-8503, Japan*

Seiya Yokogi − *Faculty of Materials Science and Engineering, Kyoto Institute of Technology, Sakyo-ku, Kyoto 606-8585, Japan*

Shinichi Sakurai − *Department of Biobased Materials Science, Kyoto Institute of Technology, Kyoto 606-8585, Japan;* orcid.org/0000-0002-5756-1066

Tomokazu Iyoda − *Division of Integrated Molecular Engineering, Chemical Resources Laboratory, Tokyo Institute of Technology, Yokohama, Kanagawa 226-8503, Japan; Faculty of Science and Engineering, Doshisha University, Kyoto 610-0394, Japan*

Complete contact information is available at: https://pubs.acs.org/10.1021/acs.macromol.5c02107

Notes

The authors declare no competing financial interest.

ACKNOWLEDGMENTS

The GIXS experiments were conducted at the Photon Factory of High Energy Accelerator Research Organization (approval# 2022G541 and 2024G587).

REFERENCES

(1) Broer, D. J.; Lub, J.; Mol, G. N. Wide-band reflective polarizers from cholesteric polymer networks with a pitch gradient. *Nature* **1995**, *378* (6556), 467−469.

(2) Chee, M. G.; Song, M. H.; Kim, D.; Takezoe, H.; Chung, I. J. Lowring Lasing Threshold in Chiral Nematic Liquid Crystal Structure with Different Anisotropies. *Jpn. J. Appl. Phys.* **2007**, *46* (5L), L437.

(3) Hwang, J.; Song, M. H.; Park, B.; Nishimura, S.; Toyooka, T.; Wu, J. W.; Takanishi, Y.; Ishikawa, K.; Takezoe, H. Electro-tunable optical diode based on photonic bandgap liquid-crystal heterojunctions. *Nat. Mater.* **2005**, *4* (5), 383−387.

(4) Uchimura, M.; Watanabe, Y.; Araoka, F.; Watanabe, J.; Takezoe, H.; Konishi, G.-i. Development of Laser Dyes to Realize Low Threshold in Dye-Doped Cholesteric Liquid Crystal Lasers. *Adv. Mater.* **2010**, *22* (40), 4473−4478.

(5) Yu, H.; Ikeda, T. Photocontrollable Liquid-Crystalline Actuators. *Adv. Mater.* **2011**, *23* (19), 2149−2180.

(6) Hird, M.; Toyne, K. J.; Goodby, J. W.; Gray, G. W.; Minter, V.; Tuffin, R. P.; McDonnell, D. G. Synthesis, mesomorphic behaviour and optical anisotropy of some novel materials for nematic mixtures of high birefringence. *J. Mater. Chem.* **2004**, *14* (11), 1731−1743.

(7) Song, Q.; Sebastian, G.; Haiqing, X.; Tson, W. S.; Yung-Ming, L.; Chin-Yen, C.; Hsu, C.-S. High birefringence lateral difluoro phenyl tolane liquid crystals. *Liq. Cryst.* **2010**, *37* (2), 139−147.

(8) Grant, B. Diacetylenic Liquid Crystals: Synthesis and Preliminary Characterization of 4,4′-Dialkyl and 4,4′-Dialkoxy Derivatives of Diphenyldiacetylene. *Mol. Cryst. Liq. Cryst.* **1978**, *48* (3−4), 175−182.

(9) Grant, B.; J, C. N.; Cox, R. J. Novel Liquid Crystalline Materials: Synthesis and preliminary characterization of new 4,4′-disubstituted diphenyldiacetylene, tolane and stilbene derivatives. *Mol. Cryst. Liq. Cryst.* **1979**, *51* (3−4), 209−214.

(10) Wu, S. T.; Finkenzeller, U.; Reiffenrath, V. Physical properties of diphenyldiacetylenic liquid crystals. *J. Appl. Phys.* **1989**, *65* (11), 4372−4376.

(11) Wu, S. T.; Meng, H. H. B.; Dalton, L. R. Diphenyl-diacetylene liquid crystals for electro-optic application. *J. Appl. Phys.* **1991**, *70* (6), 3013−3017.

(12) Arakawa, Y.; Nakajima, S.; Kang, S.; Konishi, G.-i.; Watanabe, J. Synthesis and evaluation of high-birefringence polymethacrylate having a diphenyl-diacetylene LC moiety in the side chain. *J. Mater. Chem.* **2012**, *22* (29), 14346−14348.

(13) Hwang, J. S.; Ogawa, T. ESR studies of the interaction of propagating radicals with diacetylenes. *Polym. Bull.* **1990**, *23* (2), 239−245.

(14) Burillo, G.; Ogawa, T.; Hwang, J. S. Studies on diacetylenic vinyl compounds. VI. ESR studies on the polymerization of diacetylene containing acrylate and methacrylates. *J. Polym. Sci., Part A: Polym. Chem.* **1992**, *30* (10), 2159−2164.

(15) Canizal, G.; Burillo, G.; Muñoz, E.; Gleason, R.; Ogawa, T. The interaction of poly(methacrylate) radicals with diphenyldiacetylenes. *J. Polym. Sci., Part A: Polym. Chem.* **1994**, *32* (16), 3147−3151.
(16) Lu, Y.-H.; T, T. K.; S, H. C.; Chang, H. L. Synthesis and Characterization of Side-Chain Liquid Crystalline Polymethacrylates Containing Fluorinated Diphenyldiacetylene Side-Groups. *Mol. Cryst. Liq. Cryst., A* **1994**, *250* (1), 85−97.
(17) Wang, J.-S.; Matyjaszewski, K. Controlled/living radical polymerization. atom transfer radical polymerization in the presence of transition-metal complexes. *J. Am. Chem. Soc.* **1995**, *117* (20), 5614−5615.
(18) Matyjaszewski, K.; Xia, J. Atom Transfer Radical Polymerization. *Chem. Rev.* **2001**, *101* (9), 2921−2990.
(19) Tsarevsky, N. V.; Matyjaszewski, K. "Green" Atom Transfer Radical Polymerization: From Process Design to Preparation of Well-Defined Environmentally Friendly Polymeric Materials. *Chem. Rev.* **2007**, *107* (6), 2270−2299.
(20) Matyjaszewski, K.; Tsarevsky, N. V. Nanostructured functional materials prepared by atom transfer radical polymerization. *Nat. Chem.* **2009**, *1* (4), 276−288.
(21) Georges, M. K.; Veregin, R. P. N.; Kazmaier, P. M.; Hamer, G. K. Narrow molecular weight resins by a free-radical polymerization process. *Macromolecules* **1993**, *26* (11), 2987−2988.
(22) Chiefari, J.; Chong, Y. K.; Ercole, F.; Krstina, J.; Jeffery, J.; Le, T. P. T.; Mayadunne, R. T. A.; Meijs, G. F.; Moad, C. L.; Moad, G.; et al. Living Free-Radical Polymerization by Reversible Addition−Fragmentation Chain Transfer: The RAFT Process. *Macromolecules* **1998**, *31* (16), 5559−5562.
(23) McCormick, C. L.; Lowe, A. B. Aqueous RAFT Polymerization: Recent Developments in Synthesis of Functional Water-Soluble (Co)polymers with Controlled Structures. *Acc. Chem. Res.* **2004**, *37* (5), 312−325.
(24) Moad, G.; Rizzardo, E.; Thang, S. H. Living Radical Polymerization by the RAFT Process − A Third Update. *Aust. J. Chem.* **2012**, *65* (8), 985−1076.
(25) Wegner, G. Topochemische Reaktionen von Monomeren mit konjugierten Dreifachbindungen/Tochemical Reactions of Monomers with conjugated triple Bonds. *Z. Naturforsch., B* **1969**, *24* (7), 824−832.
(26) Baughman, R. H.; Yee, K. C. Solid-state polymerization of linear and cyclic acetylenes. *J. Polym. Sci., Macromol. Rev.* **1978**, *13* (1), 219−239.
(27) Enkelmann, V. Structural aspects of the topochemical polymerization of diacetylenes. In *Polydiacetylenes*, Cantow, H.-J., Ed.; Springer Berlin Heidelberg: Berlin, Heidelberg, 1984; pp 91−136.
(28) Likhatchev, D.; Alexandrova, L.; Salcedo, R.; Ogawa, T. Topochemical polymerization of butadiynylene dibenzamides. *Polym. Bull.* **1995**, *34* (2), 149−154.
(29) Coates, G. W.; Dunn, A. R.; Henling, L. M.; Dougherty, D. A.; Grubbs, R. H. Phenyl−Perfluorophenyl Stacking Interactions: A New Strategy for Supermolecule Construction. *Angew. Chem., Int. Ed.* **1997**, *36* (3), 248−251.
(30) Donovan, K. J.; Wilson, E. G. Demonstration of high-mobility one-dimensional semiconducting polymers. *J. Phys. C* **1979**, *12* (22), 4857.
(31) Donovan, K. J.; Wilson, E. G. Demonstration of an ultra-high mobility organic polymer. *Philos. Mag. B* **1981**, *44* (1), 9−29.
(32) Spannring, W.; Bässler, H. Electron injection into a polydiacetylene crystal (DCH): Determination of electron mobility and energy level spectrum. *Chem. Phys. Lett.* **1981**, *84* (1), 54−58.
(33) Moses, D.; Heeger, A. J. Fast transient photoconductivity in polydiacetylene: carrier photogeneration, carrier mobility and carrier recombination. *J. Phys.: Condens. Matter* **1989**, *1* (40), 7395.
(34) Nishide, J.; Oyamada, T.; Akiyama, S.; Sasabe, H.; Adachi, C. High Field-Effect Mobility in an Organic Thin-Film Transistor with a Solid-State Polymerized Polydiacetylene Film as an Active Layer. *Adv. Mater.* **2006**, *18* (23), 3120−3124.
(35) Sauteret, C.; Hermann, J. P.; Frey, R.; Pradère, F.; Ducuing, J.; Baughman, R. H.; Chance, R. R. Optical Nonlinearities in One-Dimensional-Conjugated Polymer Crystals. *Phys. Rev. Lett.* **1976**, *36* (16), 956−959.
(36) Kajzar, F.; Messier, J. Cubic Nonlinear Optical Effects in Conjugated Polymers. *Polym. J.* **1987**, *19* (2), 275−284.
(37) Nakanishi, H.; Matsuda, H.; Okada, S.; Kato, M. Evaluation of nonlinear optical susceptibility of polydiacetylenes by third harmonic generation. *Polym. Adv. Technol.* **1990**, *1* (1), 75−79.
(38) Galiotis, C.; Young, R. J. The solid-state polymerization and physical properties of bis(ethyl urethane) of 2,4-hexadiyne-1,6-diol: 3. Mechanical properties. *Polymer* **1983**, *24* (8), 1023−1030.
(39) Baughman, R. H. Solid-state synthesis of large polymer single crystals. *J. Polym. Sci., Polym. Phys.* **1974**, *12* (8), 1511−1535.
(40) Matsuda, H.; Nakanishi, H.; Kato, S.-I.; Kato, M. Conductivity of polydiacetylene with π-conjugation between polymer backbone and substituents. *J. Polym. Sci., Part A: Polym. Chem.* **1987**, *25* (6), 1663−1669.
(41) Nakanishi, H.; Matsuda, H.; Okada, S.; Kato, M. *Frontiers Macromolecular Science*, Saegusa, T., Higashimura, T., Abe, A., Eds.; Wiley, 1988; p 469.
(42) Canizal, G.; Burillo, G.; Boldu, J. L.; Muñoz, E.; Ogawa, T. Radicals of Diphenylbutadiynes and Their Interactions with Diphenylpicrylhydrazyl. A Suggestion for the Nontopochemical Polymerization Mechanism of Diacetylene. *Polym. J.* **1997**, *29* (3), 230−233.
(43) Zhu, L.; Li, X.; Sanders, S. N.; Ågren, H. Unimolecular Photopolymerization of High-Emissive Materials on Cylindrical Self-Assemblies. *Macromolecules* **2015**, *48* (15), 5099−5105.
(44) Tanphibal, P.; Tashiro, K.; Chirachanchai, S. Constructing π-Electron-Conjugated Diarylbutadiyne-Based Polydiacetylene under Molecular Framework Controlled by Hydrogen Bond and Side-Chain Substituent Position. *Macromol. Rapid Commun.* **2016**, *37* (8), 685−690.
(45) Jordan, R. S.; Li, Y. L.; Lin, C.-W.; McCurdy, R. D.; Lin, J. B.; Brosmer, J. L.; Marsh, K. L.; Khan, S. I.; Houk, K. N.; Kaner, R. B.; et al. Synthesis of N = 8 Armchair Graphene Nanoribbons from Four Distinct Polydiacetylenes. *J. Am. Chem. Soc.* **2017**, *139* (44), 15878−15890.
(46) Zhu, M.; Yin, L.; Zhou, Y.; Wu, H.; Zhu, L. Engineering Rotaxane-Based Nanoarchitectures via Topochemical Photo-Cross-Linking. *Macromolecules* **2018**, *51* (3), 746−754.
(47) Lal, A.; Raju, C.; Sureshan, K. M. Supramolecular Preorganization of Amine-functionalized Diacetylene Monomers in their Crystals Allows their Topochemical Polymerization to Polydiacetylenes Capable of CO2 Capture. *Chem.—Eur. J.* **2025**, *31* (11), No. e202403935.
(48) Yang, Y.; Lee, J. Y.; Jain, A. K.; Kumar, J.; Tripathy, S. K.; Matsuda, H.; Okada, S.; Nakanishi, H. Polarization-dependent photocurrent in thin film polydiacetylene single crystals. *J. Phys.: Condens. Matter* **1991**, *3* (47), 9563.
(49) Zhu, L.; Tran, H.; Beyer, F. L.; Walck, S. D.; Li, X.; Ågren, H.; Killops, K. L.; Campos, L. M. Engineering Topochemical Polymerizations Using Block Copolymer Templates. *J. Am. Chem. Soc.* **2014**, *136* (38), 13381−13387.
(50) Hossain, M. M.; Olamilekan, A. I.; Jeong, H.-O.; Lim, H.; Kim, Y.-K.; Cho, H.; Jeong, H. D.; Islam, M. A.; Goh, M.; You, N.-H.; et al. Diacetylene-Containing Dual-Functional Liquid Crystal Epoxy Resin: Strategic Phase Control for Topochemical Polymerization of Diacetylenes and Thermal Conductivity Enhancement. *Macromolecules* **2022**, *55* (11), 4402−4410.
(51) Tian, Y.; Watanabe, K.; Kong, X.; Abe, J.; Iyoda, T. Synthesis, Nanostructures, and Functionality of Amphiphilic Liquid Crystalline Block Copolymers with Azobenzene Moieties. *Macromolecules* **2002**, *35* (9), 3739−3747.
(52) Asaoka, S.; Uekusa, T.; Tokimori, H.; Komura, M.; Iyoda, T.; Yamada, T.; Yoshida, H. Normally Oriented Cylindrical Nanostructures in Amphiphilic PEO−LC Diblock Copolymers Films. *Macromolecules* **2011**, *44* (19), 7645−7658.

https://doi.org/10.1021/acs.macromol.5c02107
Macromolecules XXXX, XXX, XXX−XXX

(53) Komura, M.; Yoshitake, A.; Komiyama, H.; Iyoda, T. Control of Air-Interface-Induced Perpendicular Nanocylinder Orientation in Liquid Crystal Block Copolymer Films by a Surface-Covering Method. *Macromolecules* **2015**, *48* (3), 672−678.
(54) Li, J.; Kamata, K.; Komura, M.; Yamada, T.; Yoshida, H.; Iyoda, T. Anisotropic Ion Conductivity in Liquid Crystalline Diblock Copolymer Membranes with Perpendicularly Oriented PEO Cylindrical Domains. *Macromolecules* **2007**, *40* (23), 8125−8128.
(55) Li, J.; Kamata, K.; Watanabe, S.; Iyoda, T. Template- and Vacuum-Ultraviolet- Assisted Fabrication of a Ag-Nanoparticle Array on Flexible and Rigid Substrates. *Adv. Mater.* **2007**, *19* (9), 1267−1271.
(56) Suzuki, S.; Kamata, K.; Yamauchi, H.; Iyoda, T. Selective Doping of Lead Ions into Normally Aligned PEO Cylindrical Nanodomains in Amphiphilic Block Copolymer Thin Films. *Chem. Lett.* **2007**, *36* (8), 978−979.
(57) Chen, A.; Komura, M.; Kamata, K.; Iyoda, T. Highly Ordered Arrays of Mesoporous Silica Nanorods with Tunable Aspect Ratios from Block Copolymer Thin Films. *Adv. Mater.* **2008**, *20* (4), 763−767.
(58) Watanabe, R.; Kamata, K.; Iyoda, T. Smart block copolymer masks with molecule-transport channels for total wet nanopatterning. *J. Mater. Chem.* **2008**, *18* (45), 5482−5491.
(59) Komiyama, H.; Komura, M.; Akimoto, Y.; Kamata, K.; Iyoda, T. Longitudinal and Lateral Integration of Conducting Polymer Nanowire Arrays via Block-Copolymer-Templated Electropolymerization. *Chem. Mater.* **2015**, *27* (14), 4972−4982.
(60) Yamamoto, T.; Kimura, T.; Komura, M.; Suzuki, Y.; Iyoda, T.; Asaoka, S.; Nakanishi, H. Block Copolymer Permeable Membrane with Visualized High-Density Straight Channels of Poly(ethylene oxide). *Adv. Funct. Mater.* **2011**, *21* (5), 918−926.
(61) Yoshida, H.; Goto, Y.; Akahori, R.; Tada, Y.; Terada, S.; Komura, M.; Iyoda, T. Slowing the translocation of single-stranded DNA by using nano-cylindrical passage self-assembled by amphiphilic block copolymers. *Nanoscale* **2016**, *8* (43), 18270−18276.
(62) Hibi, Y.; Oguchi, Y.; Shimizu, Y.; Hashimoto, K.; Kondo, K.; Iyoda, T. Self-template−assisted micro-phase segregation in blended liquid-crystalline block copolymers films toward three-dimensional structures. *Proc. Natl. Acad. Sci. U.S.A.* **2020**, *117* (35), 21070−21078.
(63) Bloor, D.; Hubble, C. L.; Ando, D. J. *Molecular Metals*; Hatfield, W. E., Ed.; Plenum, 1979; p 243.
(64) Wada, K.; Onodera, T.; Kasai, H.; Sato, R.; Takeda, Y.; Oikawa, H. Third-Order Nonlinear Optical Properties of Layered Type Hybridized Thin Films Consisting of Oriented Polydiacetylene Nanofibers and Silver Nanoparticles. *J. Phys. Chem. C* **2019**, *123* (42), 25781−25787.
(65) Barca, G. M. J.; Bertoni, C.; Carrington, L.; Datta, D.; De Silva, N.; Deustua, J. E.; Fedorov, D. G.; Gour, J. R.; Gunina, A. O.; Guidez, E.; et al. Recent developments in the general atomic and molecular electronic structure system. *J. Chem. Phys.* **2020**, *152* (15), 154102.
(66) Carriere, P.; Grohens, Y.; Spevacek, J.; Schultz, J. Stereospecificity in the Adsorption of Tactic PMMA on Silica. *Langmuir* **2000**, *16* (11), 5051−5053.
(67) Kawauchi, T.; Kawauchi, M.; Takeichi, T. Facile Synthesis of Highly Syndiotactic and Isotactic Polymethacrylates via Esterification of Stereoregular Poly(methacrylic acid)s. *Macromolecules* **2011**, *44* (4), 1066−1071.
(68) Alba-Simionesco, C.; Coasne, B.; Dosseh, G.; Dudziak, G.; Gubbins, K. E.; Radhakrishnan, R.; Sliwinska-Bartkowiak, M. Effects of confinement on freezing and melting. *J. Phys.: Condens. Matter* **2006**, *18* (6), R15.
(69) Wu, S.-T.; Hsu, C.-S.; Chen, Y.-N.; Wang, S.-R.; Lung, S.-H. Fluoro diphenyldiacetylene and tolane liquid crystals for display applications. *Opt. Eng.* **1993**, *32* (8), 1792−1797.
(70) Komura, M.; Komiyama, H.; Nagai, K.; Iyoda, T. Direct Observation of Faceted Grain Growth of Hexagonal Cylinder Domains in a Side Chain Liquid Crystalline Block Copolymer Matrix. *Macromolecules* **2013**, *46* (22), 9013−9020.
(71) Yoon, J.; Jung, S. Y.; Ahn, B.; Heo, K.; Jin, S.; Iyoda, T.; Yoshida, H.; Ree, M. Order−Order and Order−Disorder Transitions in Thin Films of an Amphiphilic Liquid Crystalline Diblock Copolymer. *J. Phys. Chem. B* **2008**, *112* (29), 8486−8495.
(72) Crihfield, A.; Hartwell, J.; Phelps, D.; Walsh, R. B.; Harris, J. L.; Payne, J. F.; Pennington, W. T.; Hanks, T. W. Crystal Engineering through Halogen Bonding. 2. Complexes of Diacetylene-Linked Heterocycles with Organic Iodides. *Cryst. Growth Design.* **2003**, *3* (3), 313−320.
(73) Tieke, B.; Lieser, G.; Wegner, G. Polymerization of diacetylenes in multilayers. *J. Polym. Sci., Polym. Chem. Ed.* **1979**, *17* (6), 1631−1644.
(74) Lieser, G.; Tieke, B.; Wegner, G. Structure, phase transitions and polymerizability of multilayers of some diacetylene monocarboxylic acids. *Thin Solid Films* **1980**, *68* (1), 77−90.
(75) Mino, N.; Tamura, H.; Ogawa, K. Analysis of color transitions and changes on Langmuir-Blodgett films of a polydiacetylene derivative. *Langmuir* **1991**, *7* (10), 2336−2341.
(76) Deckert, A. A.; Horne, J. C.; Valentine, B.; Kiernan, L.; Fallon, L. Effects of Molecular Area on the Polymerization and Thermochromism of Langmuir-Blodgett Films of Cd^{2+} Salts of 5,7-Diacetylenes Studied Using UV-Visible Spectroscopy. *Langmuir* **1995**, *11* (2), 643−649.
(77) Saito, A.; Urai, Y.; Itoh, K. Infrared and Resonance Raman Spectroscopic Study on the Photopolymerization Process of the Langmuir−Blodgett Films of a Diacetylene Monocarboxylic Acid, 10,12-Pentacosadiynoic Acid. *Langmuir* **1996**, *12* (16), 3938−3944.
(78) Fujimori, A.; Ishitsuka, M.; Nakahara, H.; Ito, E.; Hara, M.; Kanai, K.; Ouchi, Y.; Seki, K. Formation of the Newly Greenish Organized Molecular Film of Long-Chain Diynoic Acid Derivatives by Photopolymerization and Its Structural Study Using Near-Edge X-ray Absorption Fine Structure (NEXAFS) Spectroscopy. *J. Phys. Chem. B* **2004**, *108* (35), 13153−13162.

https://doi.org/10.1021/acs.macromol.5c02107
Macromolecules XXXX, XXX, XXX−XXX